Improving Task-Agnostic Energy Shaping Control of Powered Exoskeletons with Task/Gait Classification

Jianping Lin[1], *Member, IEEE*, Robert D. Gregg[2], *Senior Member, IEEE*, Peter B. Shull[1], *Member, IEEE*

***Abstract*—Emerging task-agnostic control methods offer a promising avenue for versatile assistance in powered exoskeletons without explicit task detection, but typically come with a performance trade-off for specific tasks and/or users. One such approach employs data-driven optimization of an energy shaping controller to provide naturalistic assistance across essential daily tasks with passivity/stability guarantees. This study introduces a novel control method that merges energy shaping with a machine learning-based classifier to deliver optimal support accommodating diverse individual tasks and users. The classifier detects transitions between multiple tasks and gait patterns in order to employ a more optimal, task-agnostic controller based on the weighted sum of multiple optimized energy-shaping controllers. To demonstrate the efficacy of this integrated control strategy, an in-silico assessment is conducted over a range of gait patterns and tasks, including incline walking, stairs ascent/descent, and stand-to-sit transitions. The proposed method surpasses benchmark approaches in 5-fold cross-validation ($p < 0.05$), yielding $93.17 \pm 7.39\%$ cosine similarity and $77.92 \pm 19.76\%$ variance-accounted-for across tasks and users. These findings highlight the control approach's adaptability in aligning with human joint moments across various tasks.**

***Index Terms*—Wearable Robotics, Prosthetics and Exoskeletons, Machine Learning for Robot Control.**

I. Introduction

THE advancement of robotic assistance technologies plays a critical role in enhancing the productivity of an aging workforce and improving the daily activities of individuals with mild to moderate gait impairments [1]. These exoskeletons, exemplified by the ReWalk Personal [2] and Wandercraft Atalante X [3], incorporate actuators and controllers that restrict voluntary back-driving of joints while providing substantial torque output to assist mobility impairments through kinematic control methods for walking and stair climbing [4], [5]. Although such designs are suitable for individuals with severe injuries like paraplegia, the predefined patterns employed by the controllers may not be optimal for individuals with full or residual volitional control over their limbs and conflict with the users' desired motions [5].

In response to the limitations inherent in conventional methods of exoskeleton drive and control, a novel approach is under investigation to assist individuals with residual autonomy, including those exhibiting mild to moderate gait impairments [6]–[11]. This approach revolves around the implementation of low-impedance, backdrivable systems in conjunction with pattern-free controllers. These controllers are devised to enhance voluntary human motion, counterbalance exoskeleton mass and inertia effects, and directly amplify human-induced forces [5].

Recent advances in end-to-end neural networks have enabled the instantaneous estimation of biological hip joint moments across diverse ambulatory tasks without explicitly detecting the activity, effectively making them task-agnostic [12]. However, methods that directly map kinematics to torque across a variety of tasks may have sub-optimal performance for specific tasks and users compared to models that explicitly depend on the task and user gait (e.g., via gait state estimation [13]–[16] and/or classification [17]). Incorporating memory-augmented architectures like Recurrent Neural Networks or Long Short-Term Memory Networks (LSTMs) could potentially address these challenges by maintaining state information and implicitly handling task transitions, though they require a large amount of input sequence data. Additionally, the behavior of "black-box" machine learning approaches can be unpredictable when extrapolated beyond the confines of the training dataset, requiring empirical validation for each exoskeleton application.

An alternative task-agnostic control approach uses the nonlinear control method known as energy shaping [18], [19] to augment the dynamics of the human-exoskeleton system to correspond to a new desirable Lagrangian (or Hamiltonian) energy function in closed loop. Research in [20]–[22] highlights its effectiveness in achieving task-agnostic assistance in various backdrivable lower-limb exoskeletons, while guaranteeing certain forms of passivity and stability. Underactuated systems, like exoskeletons and biped walkers, must satisfy a set of nonlinear partial differential equations (*matching conditions*) to achieve desired closed-loop dynamics. Parameterizing the control law with basis functions aligning with the feasible closed-loop dynamical structure [21] allows optimization of

Manuscript received: October 11, 2023; Revised: January 13, 2024; Accepted: June 5, 2024.

This paper was recommended for publication by Editor Pietro Valdastri upon evaluation of the Associate Editor and Reviewers' comments. The work of J. Lin and P. Shull was supported by the National Natural Science Foundation of China under Grant 52250610217. The work of R. Gregg was supported by the National Institute of Biomedical Imaging and Bioengineering of the NIH under Award Number R01EB031166. (Corresponding author: Peter B. Shull.)

[1]Jianping Lin and Peter B. Shull are with the State Key Laboratory of Mechanical System and Vibration, School of Mechanical Engineering, Shanghai Jiao Tong University, Shanghai 200240, China. (Email: jplin@ieee.org; pshull@sjtu.edu.cn).

[2]Robert D. Gregg is with the Departments of Robotics, Mechanical Engineering, and Electrical Engineering and Computer Science, University of Michigan, Ann Arbor, MI 48109, USA (Email: rdgregg@umich.edu).

Digital Object Identifier (DOI): see top of this page.

energy targets that best replicate the able-bodied joint torques from multi-activity datasets. The resulting exoskeleton controllers deliver a portion of the normative joint torque across representative activities of daily life [20]–[24].

However, by optimizing a single controller across several activities, this energy shaping approach must make compromises in torque prediction between kinematically similar activities. While constraints ensure predicted torques are always in the correct direction [21], [22], magnitudes may be reduced at certain points in the gait cycle for certain tasks. Moreover, predicting population-average joint torques does not reflect the diversity of gait patterns amongst individuals. This approach essentially sacrifices optimal task/user-specific behavior in favor of task/user flexibility, obviating the need for real-time task detection and personalization. While this presents many advantages, a novel control formulation that is both optimal and task/user-agnostic would be highly desirable.

Recognizing the complementary strengths of energy shaping and machine learning, we propose their integration in Convolutional Neural Network-based Energy Shaping (ESCNN). This integration aims to achieve both flexibility and optimality across a diverse range of tasks and users. We optimize multiple task-agnostic controllers, each prioritizing a specific user/task condition. A task/gait classifier is employed to choose a linear combination of these controllers, resulting in a biological torque predictor that accommodates a wide range of activities and individual user-specific gait patterns. This integrated approach combines energy shaping for task flexibility and Convolutional Neural Networks (CNNs) for task/user-specific optimality in exoskeleton assistance of voluntary lower-limb motion.

The rest of this paper is organized as follows. First, we revisit energy shaping control and present our machine learning integrated framework in Section II. Next, we present methods for a comparative analysis between our method and three others in Section III. Subsequently, we present simulation results and conduct statistical evaluations in Section IV. The results are interpreted and discussed in Section V.

II. Control Methods

In this section, we first provide a concise overview of the energy shaping approach presented in a prior work [21] for the human-exoskeleton system, discussing the optimization framework based on matching conditions with contact constraints. Subsequently, we introduce our novel control framework that integrates machine learning with energy shaping. This framework possesses wide applicability to various powered exoskeleton configurations, with a specific focus on knee flexion/extension dynamics estimation in the context of this study.

A. System Modelling

We analyze a biped model in the sagittal plane, featuring seven links, that represents the human-exoskeleton system. The model involves a floating stance foot and encompasses five revolute joints, as depicted in Figure 1. The inertial reference frame coincides with the heel position, (p_x, p_y), during the heel contact phase. The global heel angle ϕ is defined with respect to the vertical axis. The stance ankle, knee, and hip angles are denoted by θ_a, θ_k, and θ_h, respectively. The model's masses and moments of inertia reflect the combination of the human and exoskeleton masses.

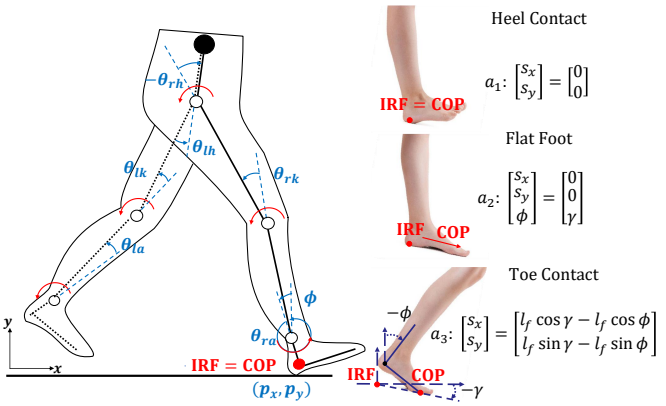

Fig. 1. Left: Kinematic model of the human body (reproduced from [21]). COP denotes Center of Pressure. Solid links denote the stance leg, and dashed links denote the swing leg. Red arcs indicate torques. Right: Heel contact (top), flat foot (center), and toe contact (bottom) during the single-support period of human locomotion. Angle γ is the ground slope, and l_f is the length of the foot. This figure is updated from [25].

To facilitate the derivation of control strategies, the dynamics of the swing and stance legs are treated distinctly, incorporating interrelated interaction forces $F = [f_x, f_y, \tau_z]^T \in \mathbb{R}^3$. The six degree-of-freedom (DOF) stance leg model has the generalized coordinates $q = [p_x, p_y, \phi, \theta_a, \theta_k, \theta_h]^T \in \mathbb{R}^6$ in the 6-dimensional configuration space $\mathscr{Q}$ (solid in Fig. 1). The conjugate momenta $p = M(q)\dot{q} \in \mathbb{R}^6$ are defined by the positive-definite inertia matrix $M(q) \in \mathbb{R}^{6\times 6}$ and the velocity vector $\dot{q}$. The port-controlled Hamiltonian dynamics can be characterized by the Hamiltonian $H(q,p) : T^*\mathscr{Q} \to \mathbb{R}$ through the equations

$$\begin{bmatrix} \dot{q} \\ \dot{p} \end{bmatrix} = \begin{bmatrix} 0 & I \\ -I & 0 \end{bmatrix} \nabla H + \begin{bmatrix} 0 \\ \tau + A^T \lambda \end{bmatrix}, \tag{1}$$

where the skew-symmetric matrix above is known as the interconnection matrix and I denotes the identity matrix. The Hamiltonian function $H(q,p) = \frac{1}{2} p^T M^{-1}(q) p + V(q)$ is given by the kinetic plus potential energy $V(q) \in \mathbb{R}$. The gradient $\nabla H = [\partial_q H, \partial_p H]^T$ is a column vector in $\mathbb{R}^{12}$ with $\partial_q H, \partial_p H \in \mathbb{R}^{1\times 6}$ as row vectors. The corresponding gravitational vector is $N = (\partial_q V)^T \in \mathbb{R}^6$. The vector of joint torques $\tau \in \mathbb{R}^6$ aggregates the human input $\tau_{\text{hum}} = Gv + J(q)^T F$ and the exoskeleton input $\tau_{\text{exo}} = Bu$, where $v \in \mathbb{R}^3$ represents the human torques (at the ankle, knee, and hip joints), and $u \in \mathbb{R}^m$ with m denotes the number of exoskeleton actuators. The inputs u and v are mapped into the overall dynamics via matrices $B \in \mathbb{R}^{6\times m}$ and $G \in \mathbb{R}^{6\times 3}$. The system is underactuated with the number of generalized coordinates larger than the number of exoskeleton actuators. The interaction forces F are mapped into the system's dynamics by the Jacobian matrix $J(q) \in \mathbb{R}^{3\times 6}$.

The holonomic contact constraints in the human-exoskeleton dynamics (Fig. 1) can be expressed as $a_\ell(q) = 0_{c\times 1}$, where c is the number of constraints and the subscript $\ell \in \{\text{heel}, \text{flat}, \text{toe}\}$ indicates the contact

configuration. The constraint matrix $A(q) = \partial_q a_\ell \in \mathbb{R}^{c\times 6}$ satisfies $A\dot{q} = A(\partial_p H)^T = 0$. The Lagrange multiplier $\lambda \in \mathbb{R}^c$ represents the ground reaction forces (GRFs) mapped into the system through constraint matrix A. Details for the contact constraints are given in [25].

B. Control Law Satisfying the Matching Conditions

Assume we have closed the feedback loop for exoskeleton input u, while the human inputs v and F remain open-loop in the Hamiltonian system. We consider a desired, closed-loop Hamiltonian $\tilde{H}(p,q) = \frac{1}{2}p^T\tilde{M}^{-1}p + \tilde{V}$, where $\tilde{V}$ represents the new potential energy. The corresponding gravitational vector is $\tilde{N} = (\partial_q \tilde{V})^T$. We set $\tilde{M} = M$ to simplify the matching conditions and to avoid complicated calculations of the inertia matrix inverse in the control law.

The desired closed-loop dynamics based on $\tilde{H}$ are

$$\begin{bmatrix}\dot{q}\\ \dot{p}\end{bmatrix} = \begin{bmatrix}0 & I\\ -I & J_2\end{bmatrix}\nabla\tilde{H} + \begin{bmatrix}0\\ Gv + J^T F + A^T\tilde{\lambda} + T_{\text{ex}}\end{bmatrix}, \quad (2)$$

where $T_{\text{ex}} \in \mathbb{R}^6$ denotes the exogenous input in [21]. The skew-symmetric matrix $J_2 = -J_2^T \in \mathbb{R}^{6\times 6}$ represents the extra shaping DOF provided in the interconnection structure [20].

Based on standard results in [19], Hamiltonian systems (1) and (2) *match* if we have

$$Bu = -(\partial_q\tilde{H})^T + (\partial_q H)^T + J_2(\partial_p H)^T + A^T(\tilde{\lambda} - \lambda) + T_{\text{ex}},$$

and the corresponding *matching condition*:

$$0 = B^\perp[-\tilde{N} + N + J_2(\partial_p H)^T + A^T(\tilde{\lambda} - \lambda) + T_{\text{ex}}], \quad (3)$$

where $B^\perp \in \mathbb{R}^{m\times 6}$ is the (full-rank) left annihilator of B, i.e., $B^\perp B = 0$. The control law for the feasible shaping structure satisfying (3) is thus

$$u = B^+[-\tilde{N} + N + J_2(\partial_p H)^T + A^T(\tilde{\lambda} - \lambda) + T_{\text{ex}}], \quad (4)$$

with $B^+ = (B^T B)^{-1}B^T$ being the left pseudoinverse of B. Details of solving matching conditions can be found in [22].

C. Energy Shaping Optimization Framework

In [21], we formed multiple basis functions for the shaping terms in (4) and optimized their coefficients to fit weight-normalized able-bodied joint torque data (given able-bodied input data) over a broad set of activities. Similarly, we can design $[-\tilde{N} + N + J_2(\partial_p H)^T + A^T(\tilde{\lambda} - \lambda) + T_{\text{ex}}]$ as a linear combination of the basis functions $\{\xi_1, \xi_2, \ldots, \xi_w\}$ with the constant coefficients $\alpha \in \mathbb{R}^w$ and verticle ground reaction forces (vGRF) scaling function $\mathscr{G}(\cdot)$, where w basis functions $\xi_i \in \mathbb{R}^6$ follow the structure of (3). The number w is determined through a grid search process. The control law (4) is thus given as

$$u = B^+\mathscr{G}(vGRF, \alpha_1\xi_1 + \cdots + \alpha_w\xi_w) = \mathscr{B}(q,p,vGRF)\alpha,$$

where $\mathscr{B}(q,p,vGRF) \in \mathbb{R}^{m\times w}$. vGRF scaling is incorporated into $\mathscr{B}(q,p,vGRF)$ via the sigmoid functions, $\frac{1}{1+e^{-a\cdot(vGRF-b)}}$. Integrating vGRF scaling divides the basis into six phases of gait cycles based on vGRF and global thigh angle values. This allows for enhanced design flexibility in aligning basis functions with normative human torques, ensuring a smooth transition between phases through the sigmoid functions.

We optimize the constant coefficients α so the outputs of control law u best fit the normalized able-bodied joint torques y. The optimization problem is defined as

$$\begin{aligned}\underset{\alpha,s}{\text{minimize}} \quad & \sum_j \mathcal{C}_j = \sum_j \Big[C_j + D_j + \mathbf{1}^T|\mathbf{S}_j| + \Lambda\|W_s\alpha\|_1\Big],\\ \text{subject to} \quad & C_j = (\mathscr{B}_j\alpha - Y_j)^T W_j(\mathscr{B}_j\alpha - Y_j),\\ & D_j = \|\bar{W}_j(\mathscr{B}_j\alpha)\|_2, \quad |\mathbf{S}_j| \geq -Y_j \odot \mathscr{B}_j\alpha,\end{aligned} \quad (5)$$

where j represents the task being optimized, $Y_j \in \mathbb{R}^{mn}$ is the normative human torque with n data samples for each task, and the matrix $\mathscr{B}_j\alpha \in \mathbb{R}^{mn}$ represents the basis evaluated at each time element along j with the state vectors $q_j, p_j \in \mathbb{R}^{n\times 6}$. Vector $\mathbf{S}_j \in \mathbb{R}^{mn}$ represents the slack for the sign difference, and $c = a \odot b$ denotes the pointwise product with $c_i = a_i b_i$.

The primary term within the optimization cost function entails the weighted square deviation between the controller torque $\mathscr{B}_j\alpha$ and the reference human torque Y_j, with consideration for the weight matrix W_j. The subsequent component seeks to minimize the temporal gradient of the controller torque, where $\bar{W}_j(i,i) = -1$ and $\bar{W}_j(i,i+1) = 1$. Another crucial element pertains to the minimization of the controller torque that opposes the direction of the reference torque Y_j, thereby ensuring that the exerted control torque aligns with the user's intended movement. To counteract overfitting, the final cost component employs L1-regularization on the parameter α, coupled with the weight matrix W_s. We solve the optimization problem using the `cvx` convex optimization package in MATLAB [26].

D. Convolutional Neural Network-based Energy Shaping (ES-CNN)

Fig. 2 illustrates the closed-loop system of the ESCNN method. In this system, machine learning enhances energy-shaping control through real-time classifications within a 500 ms sliding window, sampled at 200 Hz. These classifications serve both task recognition and gait pattern recognition to leverage customized control modules denoted as ES_i from offline energy-shaping-based optimizations with corresponding data for every combination of task and gait pattern, where $i \in \mathbb{Z} \cap [1,30]$. Tasks were categorized into six different groups, including stair ascent/descent (SA/SD), level walking (LG), ramp ascent/descent walking (RA/RD), and sit-stand cycle (SS). Note each task group includes all the variations of speed/stair heights/ramp angles. Each control module ES_i is generated through the optimization problem (5) by minimizing a combined cost of $\beta\mathcal{C}_{IG,i} + (1-\beta)\mathcal{C}_{OG,i}$, where $\mathcal{C}_{IG,i}$ is the cost associated to the specific ith task group, $\mathcal{C}_{OG,i}$ is the cost associated to task groups other than the ith group, and coefficient $\beta = 90\%$ weights the given task group in the convex sum. This optimization results in a control module ES_i that is task-agnostic across task groups but prioritizes torque prediction within its task group, accommodating inputs and outputs beyond the specified task group. The ultimate torque output furnished by the exoskeleton emerges as a linear combination of the optimal ES_i modules corresponding to

various tasks and gait patterns, where the linear coefficients (transition variables) are determined by the posterior probability from task and gait pattern recognition, adding up to 100%. Throughout the gait cycle, the controller seamlessly transitions among these optimal controllers, each tailored to specific task groups and gait patterns. The fusion of high-level classification outcomes with the energy shaping paradigm results in an adaptive controller (as long as correct task detection is not 0%), facilitating the implementation of a task-agnostic controller. Importantly, we substantiate the capabilities of this controller with empirical evidence in Section IV, demonstrating its proficiency in adeptly handling instances of misclassifications and successfully engaging in activities not explicitly covered by the training dataset.

Gait pattern recognition involves class divisions based on cosine similarity between intrasubject averaged joint torques and across-subject averaged joint torques. Class rankings were established by sorting averaged similarities across tasks per individual and categorized into five different groups in Fig. 2. For the input of the intra-stride classification, we omitted bilateral feature information to prevent the model from overfitting symmetric gait patterns. The inclusion of unilateral gait information enhances the versatility of the proposed method, making it suitable for a broader spectrum of exoskeleton configurations and improving its adaptability to real-world walking scenarios, including transitions between different walking modes. Despite the limited sensor count, the input variable dimensionality has been extended to $\mathbb{R}^{6\times100}$. This augmentation incorporates global thigh angle (ϕ), knee angle (θ_k), their respective velocities ($\dot{\phi}$ and $\dot{\theta}_k$), and the integral of global thigh angle and knee angle ($\int\phi$ and $\int\theta_k$). The inclusion of the angle's integral is inspired by previous works such as [27], [28], where the phase variable's integral is considered for gait activity classification. However, the adopted approach in these studies involves information integrated across the entire stride, which is not entirely suitable for intra-stride classification. Hence, we have adapted the integral concept from [27], [28] to $\int\phi = \int_{t-T}^{t}\phi(\tau) - \phi(t-T)d\tau$ at time t, signifying the temporal integral of the angle's change within the preceding $T = 500$ milliseconds. The initial value subtraction in this integral formulation addresses issues related to magnitude scale disparities among users and differing walking conditions.

Fig. 2 provides additional insight into the network configuration, highlighting the inclusion of 1D convolutional layers with causal padding. These layers are instrumental in acquiring data-driven feature representations, obviating manual feature engineering requirements. Following each layer, after the Rectified Linear Unit (ReLU) function, batch normalization was applied to stabilize training. Each model underwent training using the Adam optimizer. The input data consists of a window of 100 frames(a 500 ms window). This input data is structured in an $\mathbb{R}^{6\times100}$ format to facilitate temporal classifications.

E. Training Data

The training process for the energy shaping optimization and the integration of machine learning involves the utilization of normalized datasets derived from human gait information

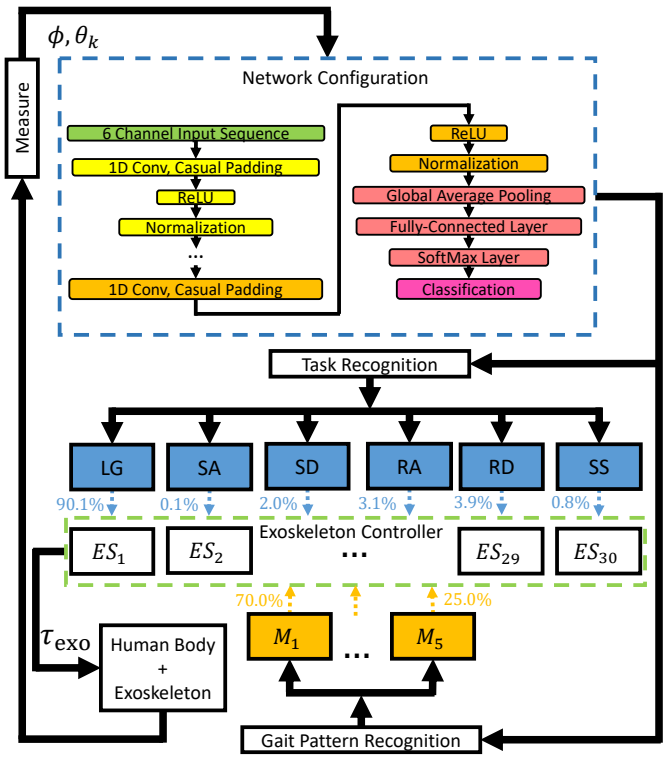

Fig. 2. Feedback loop of a human leg wearing an energy shaping exoskeleton, where τ_{exo} represents the exoskeleton input, and ϕ, θ_k, and vGRF correspond to the global thigh angle, knee joint angle, and vertical ground reaction force, respectively. The input for machine learning includes joint information ϕ and θ_k, and the output returns task categories including 'Level Ground (LG),' 'Stair Ascent/Descent (SA/SD),' 'Ramp Ascent/Descent (RA/RD),' and 'Sit-Stand cycle (SS),' along with recognition of gait patterns denoted as $M_1,\ldots,M_5$. These outputs form different energy shaping modules referred to as ES_i, where $i \in \mathbb{Z}\cap[1,30]$. The exoskeleton torques are calculated as a linear combination of the ES_i modules, with the coefficients (the possible percentages in blue and yellow) determined by the corresponding posterior probability.

of eight able-bodied subjects. This information encompasses various locomotion tasks conducted on level-ground, ramps, stairs walking [29], and stand-to-sit [30] (sit-to-stand as reverse duplicate). The joint torques in these scenarios were pre-computed through model-based estimation using inverse dynamics. In the context of locomotion tasks, vertical ground reaction forces are normalized relative to the subjects' body weight. A pragmatic assumption is employed when the stand-to-sit data from [30] lacks vertical ground reaction forces (vGRFs). Specifically, vGRFs are held at a constant value during the standing phase (a valid assumption for quasi-static activities such as stand-to-sit [31]), and they are gradually tapered down to 0 as the sitting position is approached. The compilation of training tasks encompasses a range of activities, including LL at velocities of $0.6, 1, 1.4, 1.8\text{m/s}$, RA/RD characterized by inclines of $5.2°, 7.8°, 9.2°, 11°$, SA/SD featuring step heights of $4, 5, 6, 7$inch [29], and the stand-to-sit task detailed in [30]. Each stride segment commences at the right leg heel-strike of the preceding stride and concludes at the right leg heel-strike of the subsequent stride. Comprehensive insights into the dataset are expounded in [29], [30].

III. Simulation-Based Comparison Methods

We conducted a comparative analysis between the newly proposed ESCNN approach and three existing methods,

namely the Energy Shaping (ES) method (based on only energy shaping) detailed in [21], the Long Short-Term Memory (LSTM) technique (based on only machine learning), and a state-of-art finite state machine (FSM) controller [32]. The Energy Shaping method in [21] took into account all tasks and subjects as a collective.

LSTM, categorized within the domain of recurrent neural networks, proves well-suited for temporal series regression tasks, enabling the acquisition of latent representations of historical data throughout the backpropagation process [33]. The input dataset for LSTM aligns with that of the proposed algorithm with the additional vGRFs information, encompassing raw sensor data derived from 500 ms sliding windows at time t, characterized by a dimension of $\mathbb{R}^{7\times100}$. The optimized LSTM architecture integrated a fully-connected layer for reshaping the network's output into a uniform size.

The FSM, as defined in [21], utilizes a normative able-bodied human torque from the training dataset, following a similar approach. The FSM uses a representative subject-average joint torque profile over the entire stride for each primary activity (SA/SD, RA/RD, LG, and SS), neglecting variations within each activity that would be impractical to classify. The FSM selects the nearest neighbor task from the limited task set, measured using the L2 norm. Notably, our FSM benchmark relies on a perfectly accurate oracle of the task, giving insight into the minimum possible error associated with the FSM methodology despite real-world implementation difficulties [32].

A. Neural Network Hyperparameter Optimization

A meticulous calibration of hyperparameters for both machine learning algorithms was performed to ensure a pertinent comparison across distinct control methodologies. Bayesian optimization was harnessed to identify the most fitting network hyperparameters and training configurations for the convolutional neural networks.

Regarding the hyperparameter optimization for task/gait pattern recognition, specific parameters including the count of levels (comprising two 1D convolutional layers per level), filter dimensions, quantity of filters, and the L2 regularization coefficient were subject to optimization. Similarly, the hyperparameter optimization process for the Long Short-Term Memory (LSTM) entailed the tuning of factors such as the number of LSTM cells within each hidden layer, the dropout probability, the number of layers, and the initial learning rate for the LSTM network.

B. Statistical Analysis

In evaluating our methodologies, we utilized Cosine Similarity (SIM) and Variance Accounted For (VAF) metrics to ensure the controller's efficacy. SIM $\in [-100\%, 100\%]$ assesses the alignment of the controller-generated torque patterns with normalized able-bodied torque profiles, ensuring that the exoskeleton's assistance mimics natural human movement. VAF $\in (-\infty, 100\%]$ quantifies the variability in the data and determines the extent to which the exerted control torque aligns with the user's intended movement by measuring the proportion of variance explained by our model. Together, these metrics provide a comprehensive evaluation of the controller's ability to replicate normative human joint torque while ensuring alignment with the user's movement intentions, which are defined as $\mathrm{SIM}_{A,B} = 100 \cdot \frac{A \cdot B}{\|A\|_2 \|B\|_2}$, $\mathrm{VAF}_{A,B} = 100 \cdot [1 - \frac{\mathrm{Var}(A-B)}{\mathrm{Var}(A)}]$.

To facilitate inter-method comparison, a comprehensive analysis was performed involving statistical scrutiny of SIM and VAF scores. These scores were derived from individual subjects' joint torques in conjunction with the corresponding model-predicted torques. Initial evaluation encompassed a normality assessment using the Shapiro-Wilk test. Subsequently, due to the non-normal distribution of SIM and VAF, a non-parametric analysis was adopted to ascertain the statistical impact of the control method on these metrics. For each task, pairwise comparisons were executed between modes. These comparisons employed the Wilcoxon signed-rank test, with the null hypothesis positing a zero median difference in scores between different methods.

To gauge the predictive efficacy of the proposed methodologies in the face of subject-specific and task-specific variations in joint torque, leave-one-out cross-validations were performed. First, a leave-one-subject-out cross-validation (comprising eight subjects) assessed how well the methods performed in scenarios involving subject-specific torque fluctuations. Similarly, a leave-one-task-out cross-validation (encompassing 21 tasks) was executed to evaluate the predictive competence of the proposed methodologies in instances characterized by task-specific joint torque variations. Within this validation framework, a specific ground slope, walking speed, or stair height was designated as the hold-out condition, subsequently serving as the test scenario to gauge model performance in unseen contexts. These validations clearly demonstrate the controller's effectiveness in managing misclassifications and engaging with tasks beyond the training set, underscoring its adaptability and robustness.

IV. Results

The averaged results across all tasks and gait patterns are given in Table I, where the torque prediction results of ESCNN include misclassifications, influencing the overall outcomes. The results obtained from the 5-fold cross-validation highlight the improved performance of ESCNN in terms of SIM and VAF when compared to ES, LSTM, and FSM. ESCNN task recognition yielded an average accuracy of $99.71 \pm 0.17\%$, and gait pattern recognition exhibited an average accuracy of $95.72 \pm 1.16\%$ across all tasks during testing. ESCNN demonstrated robustness to misclassified tasks—in these cases it achieved an average SIM of $90.48 \pm 5.81\%$ and an average VAF of $54.32 \pm 11.14\%$. Conversely, the ES and LSTM models do not depend on task classification, and the FSM model assumes perfect classification. In terms of estimating knee moments, the proposed method showcased a closer alignment with normative human joint torques for representative strides under steady-state ambulation conditions (Fig. 3).

To facilitate method comparison, a group statistical analysis ($n = 8$) was conducted on SIM and VAF scores derived from

TABLE I
AVERAGED RESULTS ACROSS ALL TASKS AND GAIT PATTERNS.

	ESCNN (Our Approach)	ES	LSTM	FSM
K-Fold Cross-Validation				
SIM	**93.17(7.39)**	86.91(14.62)†	82.34(11.22)†	86.91(10.72)†
VAF	**77.92(19.76)**	52.58(32.12)†	43.65(39.81)†	66.81(15.98)†
Leave-One-Subject-Out				
SIM	**87.93(18.71)**	87.04(18.47)†	83.27(21.91)†	85.99(16.85)†
VAF	**64.63(55.60)**	58.32(47.22)†	52.83(68.06)†	63.17(29.93)†
Leave-One-Task-Out				
SIM	**91.02(15.63)**	87.37(18.01)†	83.73(20.09)†	86.64(17.90)†
VAF	**73.48(42.79)**	58.81(46.27)†	61.15(44.70)†	66.16(33.95)†

† represent a statistical difference ($p < 0.05$) from ESCNN. The best performance according to SIM and VAF is bolded. Results are presented as the mean ± standard deviation in %.

each subject's joint torques, contrasted with the model's predicted torques without utilizing that subject's data. The results obtained from the leave-one-subject-out analysis highlight the improved performance of ESCNN in terms of SIM and VAF when compared to ES, LSTM, and FSM, with the exception of ramp ascent and level ground walking cases (refer to Fig. 4). ESCNN achieved an average task recognition accuracy of $95.26 \pm 5.00\%$ and an average gait pattern recognition accuracy of $75.90 \pm 18.58\%$ across all subjects. ESCNN also achieved an average SIM of $79.45 \pm 12.29\%$ and an average VAF of $51.91 \pm 25.69\%$ for the misclassified tasks.

The findings emerging from the leave-one-task-out analysis further underscore the supremacy of ESCNN, with the exception in level walking cases (Fig. 5). Notably, ESCNN achieved an average task recognition accuracy of $96.49 \pm 6.21\%$ and an average gait pattern recognition accuracy of $90.62 \pm 11.42\%$ across the excluded tasks. ESCNN also achieved an average SIM of $72.06 \pm 21.19\%$ and an average VAF of $15.61 \pm 62.26\%$ for the misclassified tasks.

V. DISCUSSION

This study introduces an energy shaping approach based on machine learning for a powered knee exoskeleton system, aimed at providing consistent support for various daily activities. As demonstrated in Section IV, the ESCNN method manifests superior performance in both similarity (how closely it matches) and variance-accounted-for (how well it accounts for variations) metrics. Despite having limited sensors, our system achieved an accuracy of over 90% in classifying both tasks and gait patterns. We verified this through 5-fold cross-validation and leave-one-subject/task-out assessments. The leave-one-subject-out analysis showed a minor reduction in gait pattern recognition, due to our gait pattern classification being dependent on torque similarity, which varies significantly among individual subjects. Excluding one subject from the analysis could result in the elimination of an entire gait pattern class. Table I reveals the ESCNN method's significant advantages over alternatives. Notably, even when tasks are misclassified, the control modes ensure the assistance torque patterns remain biomimetic, as shown by SIM, though peak values are sometimes insufficient, as noted with VAF.

Fig. 3 visually portrays the alignment of normative able-bodied knee joint torque profiles across the complete gait cycle, addressing both torque profile magnitude (VAF) and shape (SIM). Nonetheless, certain inconsistencies emerge in

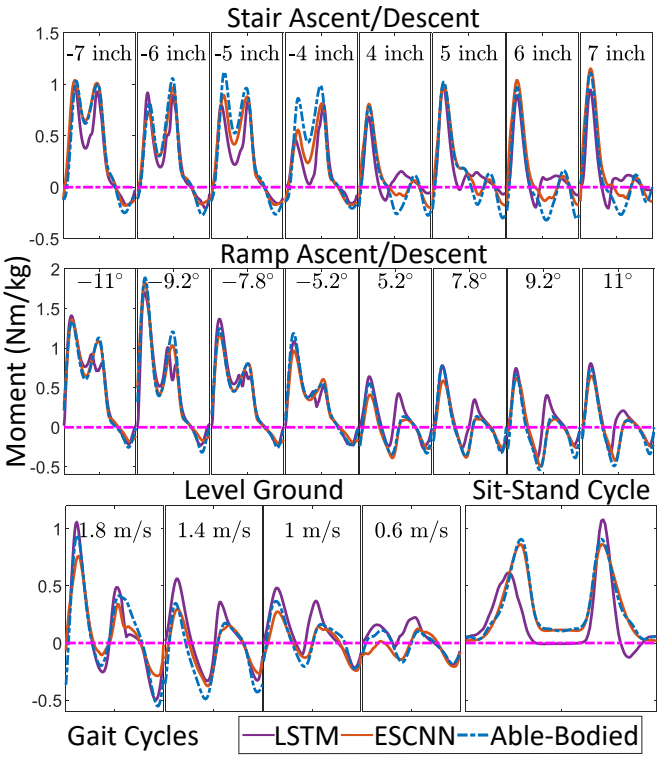

Fig. 3. Averaged results of the estimated knee joint torques and able-bodied human torques on the testing data sets. Positive values represent knee extension. The heel strike denotes the start of the gait cycle. ESCNN energy shaping and convolutional neural network, LSTM long short-term memory.

the performance of the ES and LSTM methods during specific tasks, particularly in the late stance and early swing phases. Notably, a discrepancy becomes apparent in the early stance phase at the $0.6m/s$ level walking, where all methods struggle to precisely replicate the normative human joint torque. This inconsistency can be attributed to speed variations compared to other level ground walking scenarios at higher speeds, impacting torque matching.

Collectively, ESCNN emerges as a promising avenue for delivering more biomimetic assistance in comparison to ES, LSTM, and FSM methodologies. In the 5-fold cross-validation and leave-one-subject-out evaluation, ESCNN demonstrates superior performance over alternative methods, exhibiting higher mean SIM and VAF scores across the board. As visually depicted in Fig. 4, for the 5-fold cross-validation, the discernible trend achieves statistical significance at the 0.05 significance level in all comparisons for SIM score and 16 out of 18 comparisons for VAF score. For the leave-one-subject-out evaluation, ESCNN's superior performance achieves statistical significance at the 0.05 significance level in 14 out of 18 comparisons for SIM score and 14 out of 18 comparisons for VAF score. It is noteworthy that the ES and FSM methods demonstrate exceptional performance in the context of ramp ascent, where the knee joint torques remain relatively consistent across various inclinations. However, the average joint torques generated by FSM may introduce significant variance in VAF, arising from the diverse individual joint torques observed in tasks like stair descent. In the leave-one-task-out analysis, ESCNN consistently outperforms the ES,

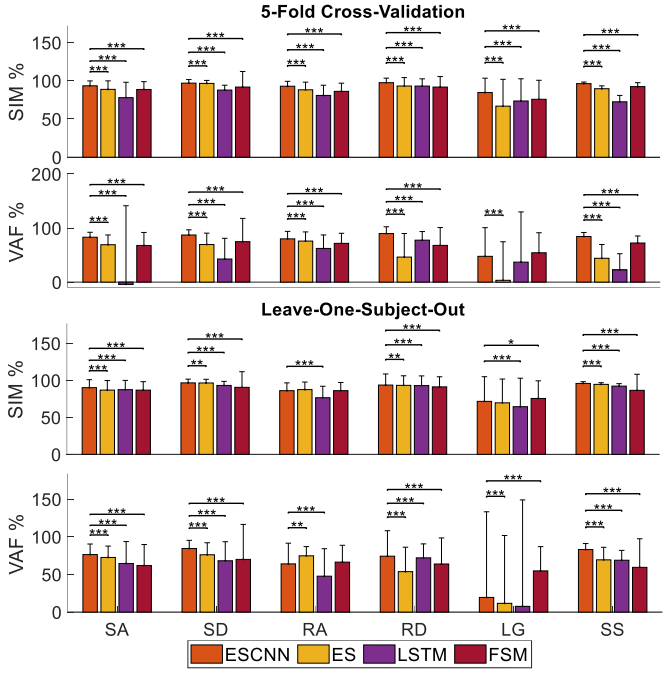

Fig. 4. Comparison of techniques for the 5-fold cross-validation (top) and leave-one-subject-out test (bottom). The error bars represent the leave-one-subject-out average ± 1 standard deviation. * represents statistical difference ($p < 0.05$). ** represents $p <= 0.01$. *** represents $p <= 0.001$. ES energy shaping, ESCNN energy shaping and convolutional neural network, LSTM long short-term memory, FSM finite state machine, SIM cosine similarity, VAF variance-accounted-for, SA/SD ascent/descent, LG level walking, RA/RD ramp ascent/descent walking, SS sit-stand cycle.

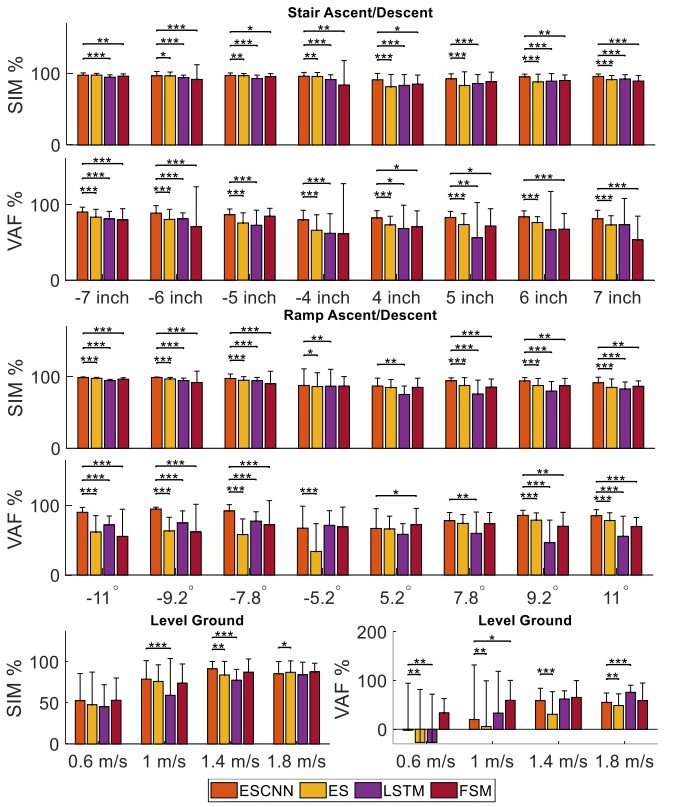

Fig. 5. Comparison of techniques for the leave-one-task-out test. The error bars represent the leave-one-task-out average ± 1 standard deviation. The number in black denotes the median. * represents statistical difference ($p < 0.05$). ** represents $p <= 0.01$. *** represents $p <= 0.001$. ES energy shaping, ESCNN energy shaping and convolutional neural network, LSTM long short-term memory, FSM finite state machine, SIM cosine similarity, VAF variance-accounted-for.

LSTM, and FSM methods in both SIM and VAF metrics across a range of lower-limb exoskeleton tasks, with the exception of level ground walking. This trend holds statistical significance at the 0.05 level in 46 out of 60 tasks for SIM score and 42 out of 60 tasks for VAF score, as visually presented in Fig. 5.

The comparatively lower performance of ESCNN in level ground walking can be attributed to the limited dataset, particularly concerning variations in walking speeds. To enhance performance, the inclusion of additional individual subjects' data in the analysis could prove advantageous. To further refine the accuracy of both task and gait pattern recognition, an increase in the sliding window size, initially set at 500 ms, shows promise. The extended sliding window enhances classification by acting as a mode transition within the energy shaping controller, substantiating task flexibility with passivity-based output torques. However, adopting a longer sliding window might introduce untimely delay issues, particularly in machine-learning-based methods like LSTM. Furthermore, the implementation of real-time sequence-to-sequence deep learning neural networks poses heightened challenges compared to the energy shaping methodology. To optimize performance in level ground walking, the optimization framework could be augmented by the inclusion of more slow-speed level ground walking tasks.

The conducted assessments within this study have focused on lower-limb exoskeleton configurations within the established control framework, with a primary focus on the knee joint. It is important to note that the proposed methodology could potentially be expanded into various unilateral and bilateral configurations, encompassing the ankle, knee, and hip joints of powered exoskeletons. Such an extension would facilitate comprehensive lower limb assistance across diverse contextual settings.

As noted in [7], an exoskeleton torque profile proportional to average biological torque may not provide optimal assistance to the user. While aiming to fit normalized able-bodied joint torques for convenient method comparison, target joint torques can be adjusted for improved assistance. Our system utilizes a backdrivable actuator with low resistive torque for human joint control. Although external torque affects walking kinematics, we assume minimal impact on subjects' walking patterns with enough adaptation time. System effects can be validated through electromyography assessments in future experiments. For real-time implementation, noise in task and gait pattern classification can be addressed by filtering and smoothing transition variables. High-level control involves task and gait pattern recognition, while the primary control kernel is the energy shaping method based on the system's feedback state. The energy shaping framework remains active, providing real-time assistance to adapt to varying speeds and conditions within task categories. Energy shaping control modes can be seamlessly switched with appropriate timings from [34], [35].

VI. Conclusion

This manuscript presents a new control framework that addresses the intricate issue of accommodating distinct individual tasks and user-specific demands within the domain of powered exoskeletons designed for augmenting everyday activities. The novel framework introduces a multi-user task-agnostic optimal energy shaping approach, capitalizing on the synergies between machine learning and energy shaping methodologies. The efficacy of the newly proposed controller is rigorously evaluated through a series of offline trials encompassing various locomotion scenarios, including walking on diverse inclines, navigating ramp ascent/descent, and executing stand-to-sit maneuvers. Comparative assessments are conducted against alternative task-agnostic control methods. Future endeavors in this line of research will involve a proof-of-concept study that incorporates multiple able-bodied subjects.

References

[1] C. Siviy, L. M. Baker, B. T. Quinlivan, F. Porciuncula, K. Swaminathan, L. N. Awad, and C. J. Walsh, "Opportunities and challenges in the development of exoskeletons for locomotor assistance," *Nat. Biomed. Eng.*, pp. 1–17, 2022.

[2] G. Zeilig, H. Weingarden, M. Zwecker, I. Dudkiewicz, A. Bloch, and A. Esquenazi, "Safety and tolerance of the rewalk™ exoskeleton suit for ambulation by people with complete spinal cord injury: a pilot study," *J. Spinal Cord Med.*, vol. 35, no. 2, pp. 96–101, 2012.

[3] O. Harib, A. Hereid, A. Agrawal, T. Gurriet, S. Finet, G. Boeris, A. Duburcq, M. E. Mungai, M. Masselin, A. D. Ames *et al.*, "Feedback control of an exoskeleton for paraplegics: Toward robustly stable, hands-free dynamic walking," *IEEE Control Syst. Mag.*, vol. 38, no. 6, pp. 61–87, 2018.

[4] T. Yan, M. Cempini, C. M. Oddo, and N. Vitiello, "Review of assistive strategies in powered lower-limb orthoses and exoskeletons," *Robot. Auton. Syst.*, vol. 64, pp. 120–136, 2015.

[5] R. Baud, A. R. Manzoori, A. Ijspeert, and M. Bouri, "Review of control strategies for lower-limb exoskeletons to assist gait," *J. Neuroeng. Rehabil.*, vol. 18, no. 1, pp. 1–34, 2021.

[6] H. Zhu, C. Nesler, N. Divekar, V. Peddinti, and R. Gregg, "Design principles for compact, backdrivable actuation in partial-assist powered knee orthoses," *IEEE/ASME Trans. Mechatron.*, 2021.

[7] T.-H. Huang, S. Zhang, S. Yu, M. K. MacLean, J. Zhu, A. Di Lallo, C. Jiao, T. C. Bulea, M. Zheng, and H. Su, "Modeling and stiffness-based continuous torque control of lightweight quasi-direct-drive knee exoskeletons for versatile walking assistance," *IEEE Trans. Robot.*, 2022.

[8] T. Zhang, M. Tran, and H. Huang, "Design and experimental verification of hip exoskeleton with balance capacities for walking assistance," *IEEE/ASME Trans. Mechatron.*, vol. 23, no. 1, pp. 274–285, 2018.

[9] S. V. Sarkisian, M. K. Ishmael, G. R. Hunt, and T. Lenzi, "Design, development, and validation of a self-aligning mechanism for high-torque powered knee exoskeletons," *IEEE Trans. Med. Robot. Bionics*, vol. 2, no. 2, pp. 248–259, 2020.

[10] J. Kim, G. Lee, R. Heimgartner, D. A. Revi, N. Karavas, D. Nathanson, I. Galiana, A. Eckert-Erdheim, P. Murphy, D. Perry, N. Menard, D. K. Choe, P. Malcolm, and C. J. Walsh, "Reducing the metabolic rate of walking and running with a versatile, portable exosuit," *Science*, vol. 365, no. 6454, pp. 668–672, 2019.

[11] C. Nesler, G. Thomas, N. Divekar, E. J. Rouse, and R. D. Gregg, "Enhancing voluntary motion with modular, backdrivable, powered hip and knee orthoses," *IEEE Robot. Autom. Lett.*, vol. 7, no. 3, pp. 6155–6162, 2022.

[12] D. D. Molinaro, I. Kang, and A. J. Young, "Estimating human joint moments unifies exoskeleton control, reducing user effort," *Science Robotics*, vol. 9, no. 88, p. eadi8852, 2024.

[13] K. Seo, Y. J. Park, J. Lee, S. Hyung, M. Lee, J. Kim, H. Choi, and Y. Shim, "Rnn-based on-line continuous gait phase estimation from shank-mounted imus to control ankle exoskeletons," in *IEEE Int. Conf. Rehabil. Robot.*, 2019, pp. 809–815.

[14] M. K. Shepherd, D. D. Molinaro, G. S. Sawicki, and A. J. Young, "Deep learning enables exoboot control to augment variable-speed walking," *IEEE Robot. Autom. Lett.*, vol. 7, no. 2, pp. 3571–3577, 2022.

[15] I. Kang, P. Kunapuli, and A. J. Young, "Real-time neural network-based gait phase estimation using a robotic hip exoskeleton," *IEEE Trans. Med. Robot. Bionics*, vol. 2, no. 1, pp. 28–37, 2019.

[16] R. L. Medrano, G. C. Thomas, C. G. Keais, E. J. Rouse, and R. D. Gregg, "Real-time gait phase and task estimation for controlling a powered ankle exoskeleton on extremely uneven terrain," *IEEE Trans. Robot.*, 2023.

[17] I. Kang, D. D. Molinaro, G. Choi, J. Camargo, and A. J. Young, "Subject-independent continuous locomotion mode classification for robotic hip exoskeleton applications," *IEEE. Trans. Biomed. Eng.*, vol. 69, no. 10, pp. 3234–3242, 2022.

[18] A. M. Bloch, N. E. Leonard, and J. E. Marsden, "Stabilization of mechanical systems using controlled lagrangians," in *IEEE Conf. Decis. Control*, vol. 3, 1997, pp. 2356–2361.

[19] R. Ortega, A. Loría, P. J. Nicklasson, and H. J. Sira-Ramirez, *Passivity-based control of Euler-Lagrange systems*. Springer-Verlag, 1998.

[20] J. Lin, N. V. Divekar, G. Lv, and R. D. Gregg, "Optimal task-invariant energetic control for a knee-ankle exoskeleton," *IEEE Control Syst. Lett.*, 2021.

[21] J. Lin, N. V. Divekar, G. C. Thomas, and R. D. Gregg, "Optimally biomimetic passivity-based control of a lower-limb exoskeleton over the primary activities of daily life," *IEEE Open J. Control Syst.*, vol. 1, pp. 15–28, 2022.

[22] J. Lin, G. C. Thomas, N. V. Divekar, V. Peddinti, and R. D. Gregg, "A modular framework for task-agnostic, energy shaping control of lower-limb exoskeletons," *TechRxiv*, 2023. [Online]. Available: https://doi.org/10.36227/techrxiv.24487378.v1

[23] J. Zhang, J. Lin, V. Peddinti, and R. D. Gregg, "Optimal energy shaping control for a backdrivable hip exoskeleton," in *American Control Conference*. IEEE, 2023.

[24] K. Walters, G. C. Thomas, J. Lin, and R. D. Gregg, "An energetic approach to task-invariant ankle exoskeleton control," in *2023 IEEE/RSJ Int. Conf. Intell. Robots Syst.* IEEE, 2023.

[25] G. Lv, H. Zhu, and R. D. Gregg, "On the design and control of highly backdrivable lower-limb exoskeletons: A discussion of past and ongoing work," *IEEE Control Syst. Mag.*, vol. 38, no. 6, pp. 88–113, 2018.

[26] M. Grant and S. Boyd, "CVX: Matlab software for disciplined convex programming, version 2.1," http://cvxr.com/cvx, Mar. 2014.

[27] H. L. Bartlett and M. Goldfarb, "A phase variable approach for imu-based locomotion activity recognition," *IEEE Trans. Biomed. Eng.*, vol. 65, no. 6, pp. 1330–1338, 2017.

[28] X. Tan, B. Zhang, G. Liu, X. Zhao, and Y. Zhao, "Phase variable based recognition of human locomotor activities across diverse gait patterns," *IEEE Trans. Human-Machine Systems*, vol. 51, no. 6, pp. 684–695, 2021.

[29] J. Camargo, A. Ramanathan, W. Flanagan, and A. Young, "A comprehensive, open-source dataset of lower limb biomechanics in multiple conditions of stairs, ramps, and level-ground ambulation and transitions," *J. Biomech.*, vol. 119, p. 110320, 2021.

[30] B. Laschowski, R. S. Razavian, and J. McPhee, "Simulation of stand-to-sit biomechanics for robotic exoskeletons and prostheses with energy regeneration," *IEEE Trans. Med. Robot. Bionics*, vol. 3, no. 2, pp. 455–462, 2021.

[31] B. Etnyre and D. Q. Thomas, "Event standardization of sit-to-stand movements," *Physical therapy*, vol. 87, no. 12, pp. 1651–1666, 2007.

[32] M. R. Tucker, J. Olivier, A. Pagel, H. Bleuler, M. Bouri, O. Lambercy, J. del R Millán, R. Riener, H. Vallery, and R. Gassert, "Control strategies for active lower extremity prosthetics and orthotics: a review," *J. Neuroeng. Rehabil.*, vol. 12, no. 1, pp. 1–30, 2015.

[33] D. D. Molinaro, I. Kang, J. Camargo, M. C. Gombolay, and A. J. Young, "Subject-independent, biological hip moment estimation during multimodal overground ambulation using deep learning," *IEEE Trans. Med. Robot. Bionics*, vol. 4, no. 1, pp. 219–229, 2022.

[34] F. Zhang, M. Liu, and H. Huang, "Investigation of timing to switch control mode in powered knee prostheses during task transitions," *PLOS one*, vol. 10, no. 7, p. e0133965, 2015.

[35] S. Cheng, E. Bolívar-Nieto, C. G. Welker, and R. D. Gregg, "Modeling the transitional kinematics between variable-incline walking and stair climbing," *IEEE Trans. Med. Robot. Bionics*, vol. 4, no. 3, pp. 840–851, 2022.